RSC Advances

PAPER

View Article Online
View Journal | View Issue

Cite this: *RSC Adv.*, 2023, **13**, 7703

Gadolinium-based Sm^{3+} activated $GdSr_2AlO_5$ nanophosphor: synthesis, crystallographic and opto-electronic analysis for warm wLEDs

Pawan Kumar, Devender Singh * and Isha Gupta

A material's luminosity characteristics, which in turn dictate its applicability, are critically influenced by its structure. Therefore, it is essential for design and fabrication of optical nanocrystalline materials to comprehend the relationship between structural and luminescence properties. The gel-combustion approach was used to produce a sequence of orange–red light emanating $GdSr_2AlO_5:Sm^{3+}$ (GSA:Sm^{3+}) nanophosphors which are used for warm white-light-emitting diodes (w-LEDs). Comprehensive investigation of the structural and optical characteristics of $GdSr_2AlO_5:Sm^{3+}$ nanophosphors has been done in a detailed manner. The synthesized powdered nanophosphors are crystallized in a tetragonal phase with *I*4/*mcm* (140) space group, affirmed through Rietveld refining method. The nano size with an aggregated, spherical form of the particles in the powdered nanocrystalline material was revealed by TEM analysis. These orange–red emitting phosphors $Gd_{1-x}Sr_2AlO_5:xSm^{3+}$ ($x = 1$–7 mol%) were shown to possess photoluminosity (PL) properties that demonstrated the presence of most intense emission peaks at 603 nm that were caused by $^4G_{5/2} \rightarrow {}^6H_{7/2}$ transitions of the Sm^{3+} ion under 273 nm excitation. Considering its long decay lifespan and PL emission, it can be concluded that the $GdSr_2AlO_5:Sm^{3+}$ phosphor is a potential single element for the fabrication of warm white light-emitting devices.

Received 30th January 2023
Accepted 24th February 2023

DOI: 10.1039/d3ra00636k

rsc.li/rsc-advances

1 Introduction

Due to an overpopulation problem and individuals choosing to live opulent lifestyles, there has been a significant increase in global energy demand and consumption. Two important strategies *viz.* energy-saving tactics and utilizing green, renewable energy can be used to address the energy demand and consumption issues.[1–5] Researchers are fascinated by a class of rare earth doped nanophosphors in this emerging era of nanotechnology because of its implications in field emission displays (FED),[6] white light emitting diodes (wLEDs),[7–9] plasma displays (PD)[10,11] and opto-electronic devices.[12–14] Due to their intriguing properties, such as their strong luminescence reliability, spectacular chemical stability, and adaptable emission color accompanied by a variety of activators, these sorts of nanophosphors are extensively researched.[15,16] The wLEDs have been steadily replacing conventional incandescent and fluorescent lamps to become the predominant light sources in our everyday lives because of their high luminous efficiency, long lifespan and energy economy.[17–19] However, the current state of commercial wLEDs is still poor due to the absence of a suitable red component, which results in a low color rendering index and subpar light output.[20,21] Thus, the creation of novel red phosphors useful for WLEDs is still a significant and pressing subject, one that is gaining more and more attention in the solid state lighting (SSL) field.[22]

Simply a minor extent of rare earth (RE) ions might significantly alter the phase, stability and photo-physical characteristics of host semiconductor nanoparticles. These doped systems are currently regarded as a crucial class of optoelectronic materials because they can produce dopant light that is effective, stable, and controllable.[23,24] Therefore, adopting a host material with exceptional luminescence efficiency qualities is essential for the design and development of innovative optical materials. Gadolinium based $GdSr_2AlO_5$ (GSA) is assumed to be a best host material because of its good magnetic and luminescent characteristics which would be substantial and expressive for the potential application in lighting field. $GdSr_2AlO_5$ (GSA) is crystallized into tetragonal crystal structure with space group *I*4/*mcm*.[25] In the unit cell ($Z = 4$) of $GdSr_2AlO_5$, Gd and one Sr atom surrounded with 8 oxygen-atoms, second Sr atom surrounded with ten oxygen-atoms and Al atoms form tetrahedral with four oxygen atoms.[26] Eu^{3+}-doped red phosphors are typically thought of as the optimum red components for wLEDs, however using pricey Eu sources makes it difficult to realize low-cost lighting applications. So, in RE family, Sm^{3+} ion having the usual f–f electronic-transitions are commonly used as effective dopant for orange/red visible light in host matrix.[27] To investigate novel red nanophosphor modules for wLEDs, further more research on Sm^{3+} doped inorganic material has been dynamically launched. Largely, the classic solid-state

Department of Chemistry, Maharshi Dayanand University, Rohtak, 124001, Haryana, India. E-mail: devjakhar@gmail.com

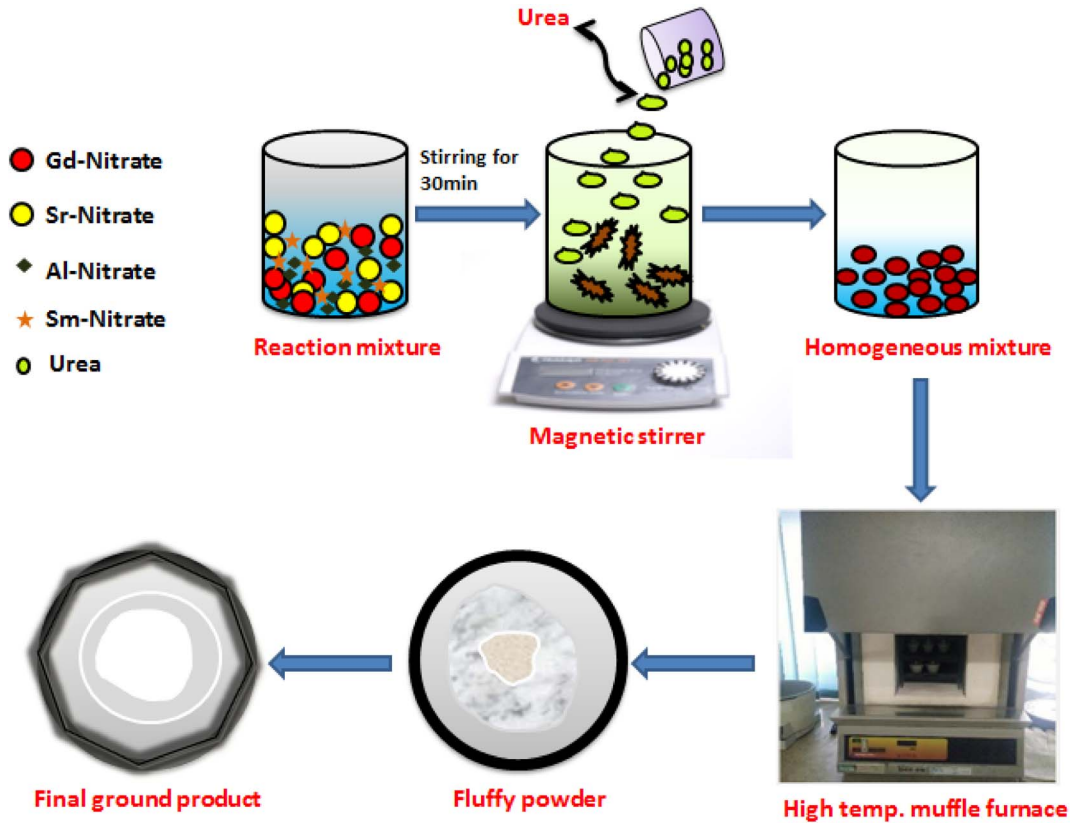

Fig. 1 Schematic diagram of GC method for the synthesis of $Gd_{1-x}Sr_2AlO_5:xSm^{3+}$ (x = 1–7 mol% Sm^{3+}) nanopowders.

reaction (SSR) technique is typically used to develop nano-phosphor. This method often involves a lengthy, high-temperature heating procedure followed by grinding. The phosphor surfaces are degraded during the grinding process, which reduces the intensity of the emission. Additionally, the product is easily able to include many impurity phases due to

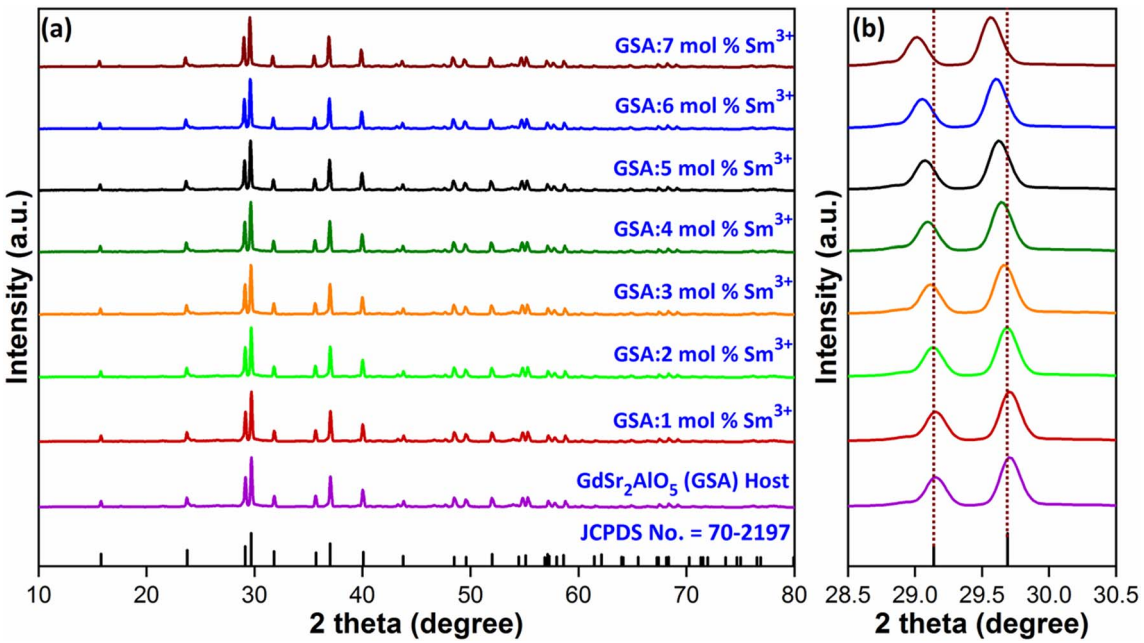

Fig. 2 (a) Diffraction profiles of $GdSr_2AlO_5$ and $Gd_{1-x}Sr_2AlO_5:xSm^{3+}$ (x = 1–7 mol% Sm^{3+}) phosphors (b) enlarged view of respective diffraction patterns.

Table 1 Computed interplaner *d*-spacing values of GSA:xSm^{3+} (x = 1–7 mol%) phosphors

Sample	2θ-value	*d*-spacing value (Å)
GSA:0 mol% Sm^{3+}	29.70	3.0056
GSA:1 mol% Sm^{3+}	29.69	3.0066
GSA:2 mol% Sm^{3+}	29.67	3.0087
GSA:3 mol% Sm^{3+}	29.66	3.0095
GSA:4 mol% Sm^{3+}	29.64	3.0115
GSA:5 mol% Sm^{3+}	29.61	3.0144
GSA:6 mol% Sm^{3+}	29.59	3.0165
GSA:7 mol% Sm^{3+}	29.56	3.0194

inadequate mixing and poor reactivity of the basic ingredients. The phosphor precursor is recently prepared using a variety of wet chemical processes, including co-precipitation,[28] sol–gel,[29] combustion,[30] hydrothermal[31] and solvothermal.[32]

Due to its benefits in producing novel chemical compositions with distinctive properties, excellent purity, smaller particle sizes and relatively low reaction temperature leading to more homogeneous products, the gel-combustion process has recently attracted a lot of devotion among synthetic approaches.[33,34] We are aware of no significant reports in the literature regarding the crystallography and opto-electronic characteristics of $GdSr_2AlO5:Sm^{3+}$ nanophosphors produced *via* the gel-combustion process. Therefore, in the present work, $Gd_{1-x}Sr_2AlO_5$:xSm^{3+} (x = 1–7 mol%) phosphors have been fabricated by gel-combustion process. The diffraction, transmission electron microscope (TEM), EDX and photoluminescence spectroscopy have been engaged to illustrate the samples. The photoluminescence properties of $GdSr_2AlO_5:Sm^{3+}$ were studied in detail, including excitation and emission spectra and CIE color coordinates. Additionally, the possible energy transfer mechanism from Gd^{3+} to Sm^{3+} on tuning of the down-conversion emission properties and lifetime decay investigation of the considered samples were discussed and concluded.

2 Experimental

2.1 Synthesis and instrumentations

A series of $Gd_{1-x}Sr_2AlO_5$:xSm^{3+} (x = 1–7 mol%) powder samples were produced using a gel-combustion approach (Fig. 1). According to the chemical formulae, stoichiometric amounts of high grade chemicals of Sigma Aldrich, such as Gadolinium Nitrate Hexahydrate [$Gd(NO_3)_3\cdot 6H_2O$; 99.9% pure] and Samarium Nitrate Hexahydrate [$Sm(NO_3)_3\cdot 6H_2O$; 99.9% pure], Aluminium Nitrate Nonahydrate [$Al(NO_3)_3\cdot 9H_2O$; 99.9% pure], Strontium nitrate [$Sr(NO_3)_2$; 99.9% pure] and Urea [NH_2CONH_2] have been used as raw materials. Double distilled (DD) water has been utilised as a solvent. Primarily, precursor were taken in measured stoichiometry and liquefied completely in solvent (deionized water). Upon warming at ~80 °C, this prepared mixture was converted to viscous form due to vaporization of solvent molecules. Then, a measured amount of fuel (urea) with

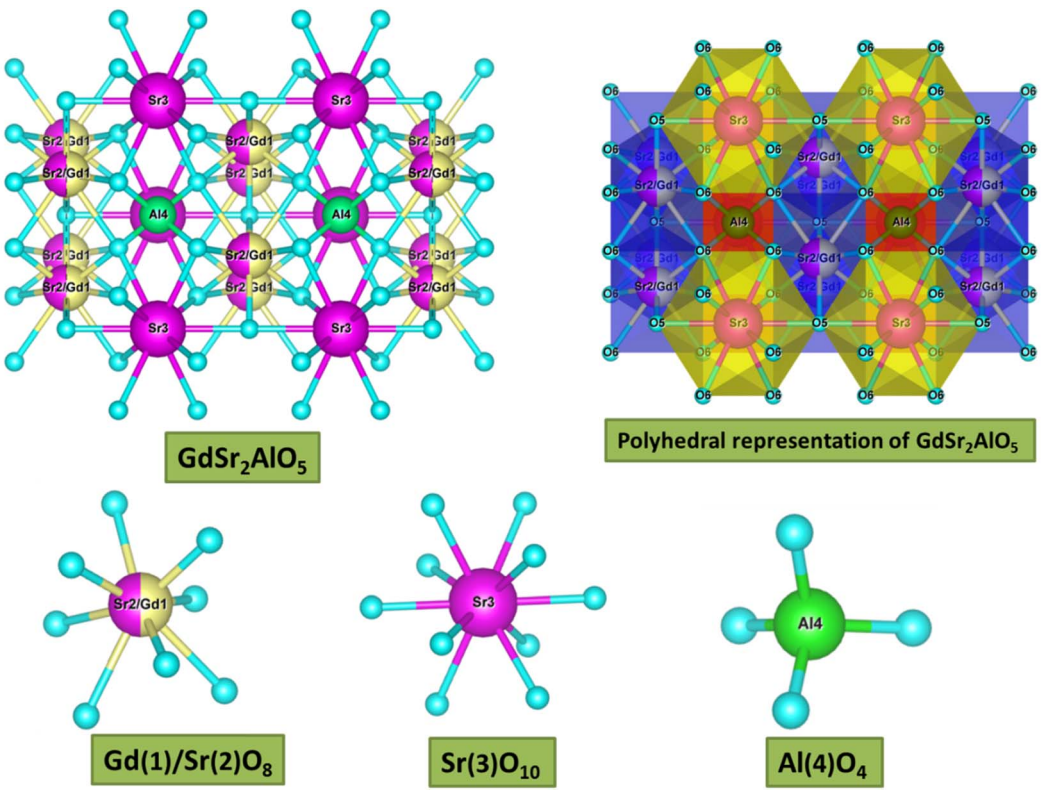

Fig. 3 3-D structural view of host $GdSr_2AlO_5$ sample along with coordinative environment of different cations.

deionized (DI) water has been added to resulting viscous solution and further heated. The formed gel type mixture was allowed to combust for fifteen minutes in a furnace which is already heated at 600 °C. In this one step preparation technique, gaseous products *viz.*, oxides of carbon and nitrogen excluded out during combustion.[35] The low temperature of reaction is answerable for development of nano-crystalline materials. This combustion method is exothermic in nature

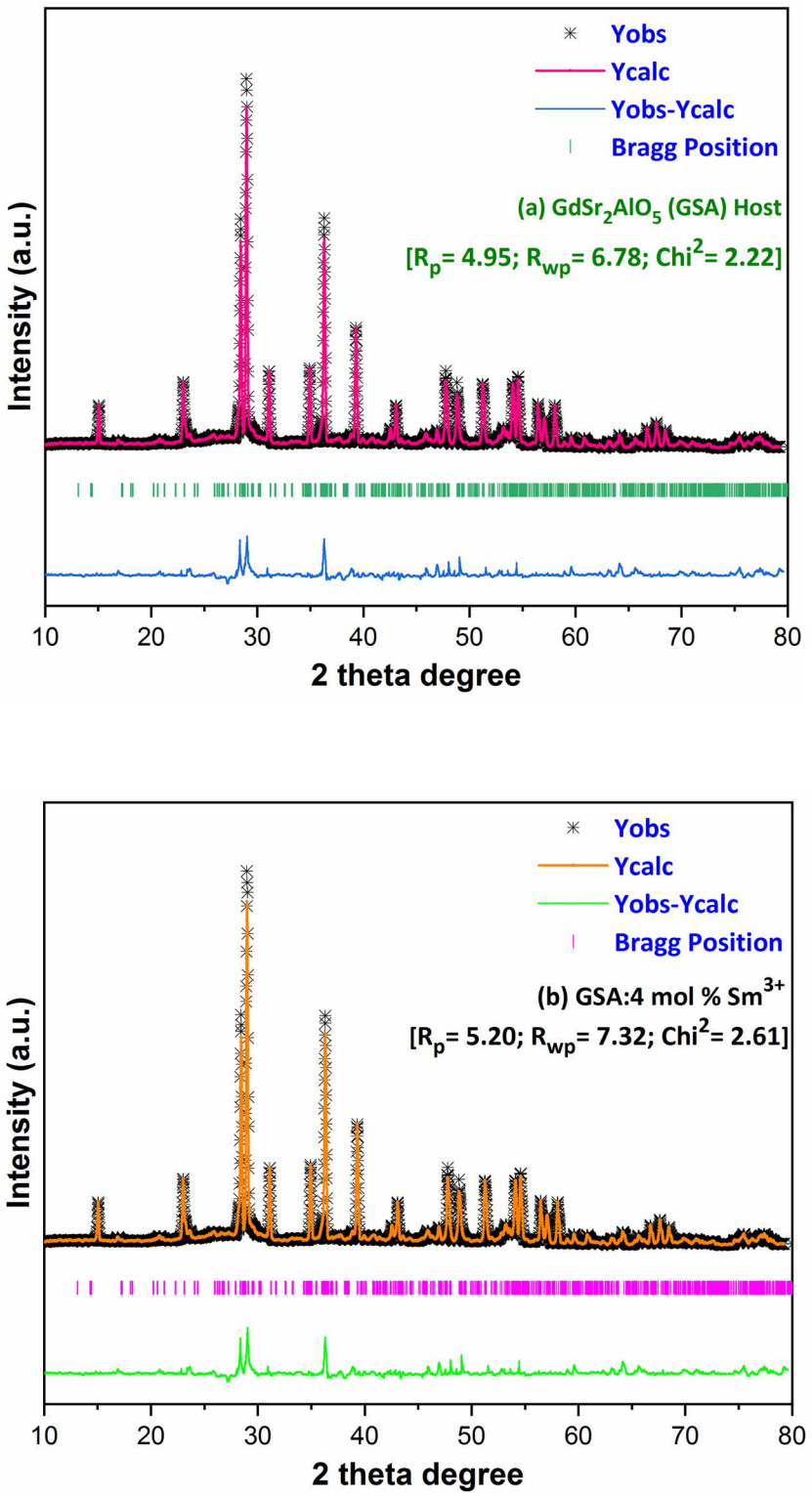

Fig. 4 Rietveld profiles of (a) $GdSr_2AlO_5$ and (b) Sm^{3+} (4 mol%) doped $GdSr_2AlO_5$ phosphors.

which results in excessive crystallinity of produced materials. The product formed is porous in nature was allowed to cool and successive grinding of product to obtain fine crushed material. The formed powdered sample was further calcined at 1350 °C in the muffle-furnace to obtain desired product.

The engineered nanosamples were studied *via* diverse techniques at normal conditions. Phase and other crystal parameters were explored by operating on Rigaku Ultima-IV X-ray diffractometer (with Cu-Kα-radiation; wavelength is 0.15405 nm, current is 40 mA, voltage is 40 kV) with a step-width of 0.02° and scanning-frequency 2° per minute. The shape and size of the particle were inspected by TECNAI TEM (field-emission gun of 200 kV). Ametek-energy-dispersive X-ray spectrometer was employed for recording EDX profiles for elemental investigation. The reflectance spectra of phosphors have been noted on a UV-3600 Plus, Shimadzu Spectrophotometer for locating optical band data gap. Horiba Fluorolog (Jobin YVON) spectrophotometer was operated for achieving the photoluminescence individualities of nano-particles by recording spectral profiles on it.

3 Results and discussion

3.1 Analysis of crystal phase and structure

Diffraction exploration was used to complete the crystalline structure examination and the final $Gd_{1-x}Sr_2AlO_5$:xSm^{3+} (x = 1–7 mol%) samples were determined to be compatible with the normal host $GdSr_2AlO_5$ matrix framework and well indexed with standard patterns (JCPDS number 70-2197),[36] as displayed in Fig. 2(a). This finding indicates that no rare earth ion peak or secondary phase residues can be identified in the XRD graph. Hence, materials created by synthesis are made of single phase. However, in the present case, there is peak shifting mechanism was observed. The position of the diffraction peak shifted to the left, as indicated in the Fig. 2(b), in accordance with the Bragg diffraction hypothesis $2d\sin\theta = n\lambda$.[37] The θ-value decreased because the radius of the doped ions (Sm^{3+}) was bigger, which increased the value d-spacing, listed in Table 1. The $GdSr_2AlO_5$ crystal lattice is composed of $GdSrO^{3+}$ and $SrAlO_4{}^{3+}$ layers, as displayed in Fig. 3. Around the rare earth ion Gd^{3+} at the half 8 h position are eight oxygen atoms forming GdO_8 polyhedron. Two distinct crystallographic locations exist for the alkaline earth ion Sr^{2+}: 8 h (Sr1) and 4a (Sr2). Sr1 atoms are positioned to place the other half of the 8 h sites, and Sr2 atoms are nearby to create 10-fold coordinated polyhedra. There are three lattice-sites with two different valences that are evidently available for the assimilation of samarium ion.[38] The incoming activator Sm^{3+} ions are thought to enter in Gd^{3+} sites. To further support the idea that the Sm^{3+} ion may be readily integrated into the GSA host, which is described as the following (eqn (1)), the percentage difference of radius (Dr) should be examined.[39]

$$D_r = \frac{R_h(CN) - R_d(CN)}{R_h(CN)} \times 100\% \quad (1)$$

here, the radius of Sm^{3+} ion (R_d) is 1.079 Å when the coordinate number (CN) is 8. The radius of the possible substituted Gd^{3+} ion (R_h) was equal to be 1.053 Å (CN = 8). Moreover, because of the balance of chemical valence, the incoming Sm^{3+} ions would substitute the Gd^{3+} ion locations. When CN = 8, it was simple to compute the percentage difference in radius (Dr) between the Sm^{3+} and Gd^{3+} ions to be around −2.46%, which is significantly less than 30%,[40] further indicating that the activator Sm^{3+} ion would occupy the host Gd^{3+} ions positions. Additionally, it is exposed through refinement process that every sample in the synthesized Sm^{3+} series has a pure tetragonal crystal structure having *I*4/*mcm* (140) space group symmetry. As a result, it can be concluded that the combustion-derived products are extremely pure and do not alter with variations in Sm^{3+} concentration. With the use of crystallographic data of GSA and Sm^{3+} (4 mol%) doped GSA samples, the refinement findings with R_p = 4.95% and 6.78%, R_{wp} = 5.20% and 7.32%, χ^2 = 2.22 and 2.61, respectively. The refined profile of GSA and Sm^{3+} (4 mol%) doped GSA samples are displayed in Fig. 4 (a and b). Table 2 shows the comparative refinement results of synthesized host and optimal doped phosphors. Table 3 listed the well-refined atomistic locations and displacement characteristics of host material. Scherrer's-relation, shown in eqn (2) was used to calculate the crystallite size of the fabricated samples.[41]

$$D_{hkl} = \frac{k\lambda}{\beta(2\theta)\cos\theta} \quad (2)$$

here, X-ray wavelength is symbolized as λ, diffraction angle is denoted with θ, and most intense peak's full width at half maximum (radians) is denoted with β. For the crystalline nanosamples of $GdSr_2AlO_5$ and $Gd_{1-x}Sr_2AlO_5$:xSm^{3+} (x = 1–

Table 2 Crystallographic parameters for $GdSr_2AlO_5$ and optimal $Gd_{0.96}Sr_2AlO_5$:4 mol% Sm^{3+} nanophosphors

Sample	$GdSr_2AlO_5$	$Gd_{0.96}Sr_2AlO_5$:4 mol% Sm^{3+}
Crystal system	Tetragonal	Tetragonal
Lattice symbol	I	I
Space group	*I*4/*mcm*	*I*4/*mcm*
Pearson symbol	tI	tI
Centro-symmetry	Centric	Centric
Formula unit (Z)	4	4
Space group number	140	140
$\alpha = \beta = \gamma$	90.0000	90.0000
a (Å)	6.88630	6.89217
b (Å)	6.88630	6.89217
c (Å)	11.04070	11.07214
Volume (Å^3)	523.562	525.948
R-factors	4.95, 6.78	5.20, 7.32
χ^2	2.22	2.61

Table 3 The atomistic and equivalent isotropic displacement parameters of host $GdSr_2AlO_5$

Atom	x	y	z	W_{yck}	U	Occ	Sym
Gd1	0.17951	0.67951	0.00000	8h	0.006	0.500	m.2 m
Sr2	0.17951	0.67951	0.00000	8h	0.006	0.500	m.2 m
Sr3	0.00000	0.00000	0.25000	4a	0.006	1.000	422
Al4	0.00000	0.50000	0.25000	4b	0.009	1.000	−42 m
O5	0.00000	0.00000	0.00000	4c	0.012	1.000	4/m..
O6	0.14343	0.64343	0.64207	16l	0.012	1.000	..m

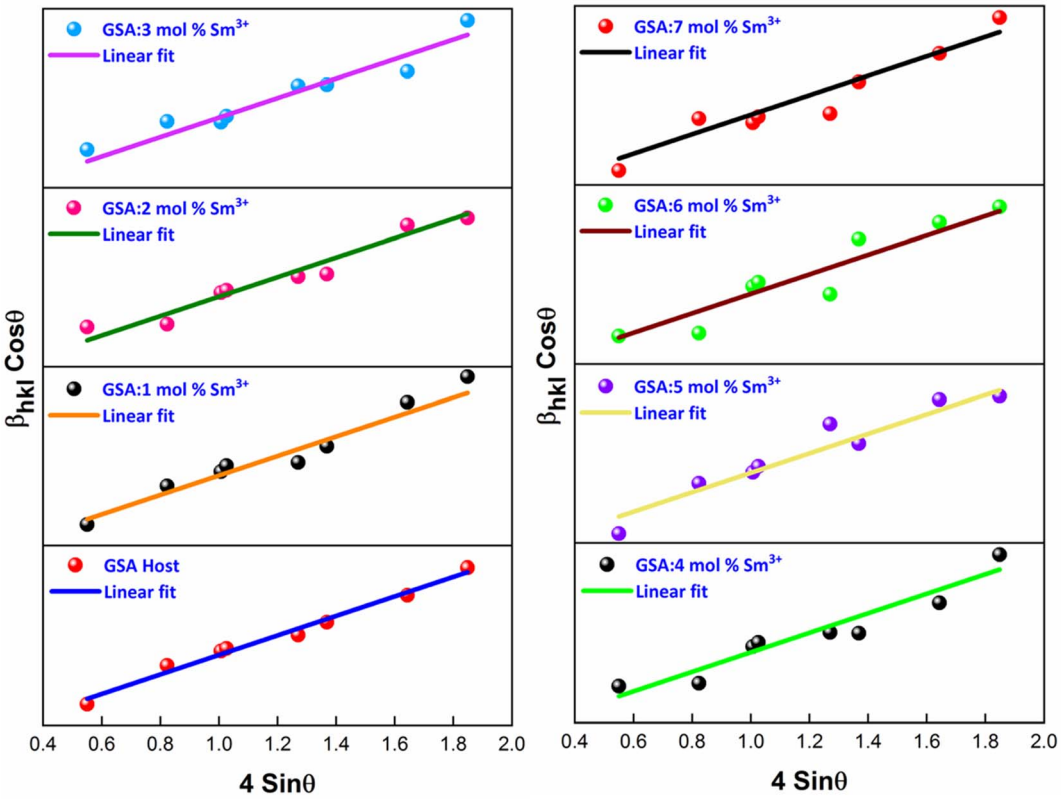

Fig. 5 W–H plots of $Gd_{1-x}Sr_2AlO_5$:xSm^{3+} (x = 1–7 mol% Sm^{3+}) phosphors.

Table 4 XRD characteristics of host GSA and GSA:xSm^{3+} (x = 1–7 mol% Sm^{3+}) phosphors

Sample	FWHM	Crystallite size (nm)		Microstrain ($\varepsilon \times 10^{-4}$)
		Scherrer's	W–H	
GSA:0 mol% Sm^{3+}	0.2368	34.71	43.29	5.2314
GSA:1 mol% Sm^{3+}	0.2403	34.20	41.11	5.7890
GSA:2 mol% Sm^{3+}	0.2479	33.15	40.24	5.9504
GSA:3 mol% Sm^{3+}	0.2561	32.09	39.03	6.2896
GSA:4 mol% Sm^{3+}	0.2633	31.21	37.89	7.2560
GSA:5 mol% Sm^{3+}	0.2682	30.64	36.28	7.7221
GSA:6 mol% Sm^{3+}	0.2733	30.07	35.48	7.9730
GSA:7 mol% Sm^{3+}	0.2819	29.16	34.87	8.5634

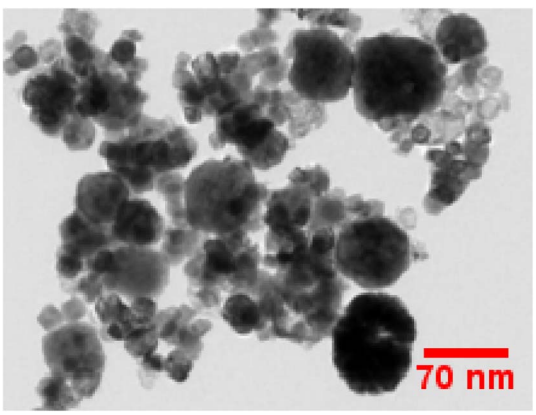

Fig. 6 TEM micrograph of as-prepared $Gd_{0.96}Sr_2AlO_5$:4 mol% Sm^{3+} phosphors.

7 mol%), the crystallite size was possibly estimated to be in between 29–35 nm. Diffractograms show peak shifting and line broadening due to the presence of micro-strain in crystallized nanomaterial. Thus, the strain existing in the investigated nanosamples was evaluated by utilizing eqn (3) employing W–H linear fitting approach.[42]

$$\beta_{hkl} \cos \theta_{hkl} = \frac{K\lambda}{D} + 4\varepsilon \sin \theta_{hkl} \quad (3)$$

The W–H plot (Fig. 5) reveals that the graph between 4 sin θ_{hkl} v/s cos θ_{hkl} indicates a straight line. The linear fitted profile's slope and intercept values perfectly capture ε and D values of the sample. All manufactured samples have different crystallite sizes that vary within 34–40 nm. It has been revealed that the crystallite sizes derived by using W–H plots are larger than those obtained by the Debye Scherrer's formula. It has been due to the strain component that influences the produced nanocrystalline materials is the primary reason of this minimal variation. The determined outcomes are concise in Table 4.

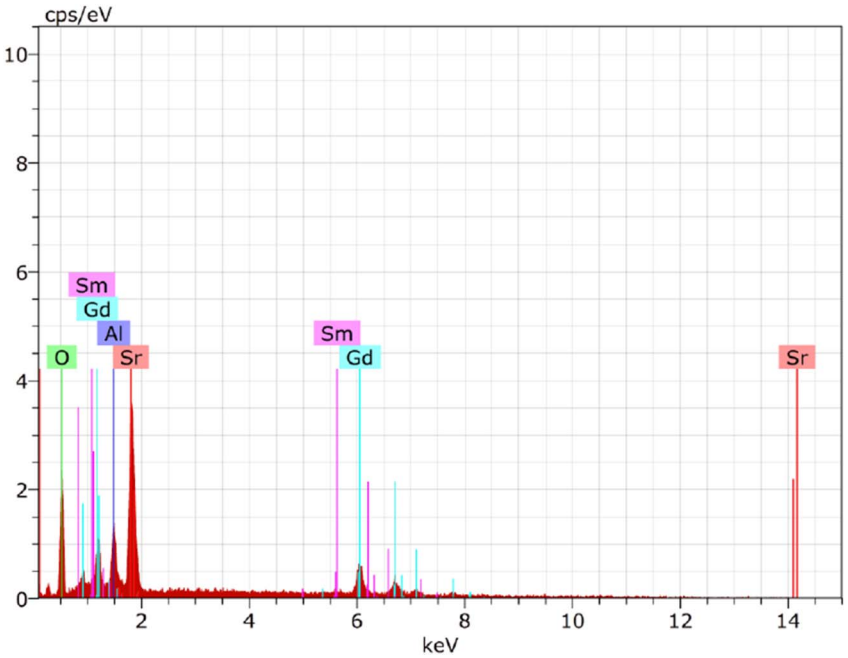

Fig. 7 EDX spectrum of as-prepared $Gd_{0.96}Sr_2AlO_5$:4 mol% Sm^{3+} phosphors.

Table 5 Atomic & Weight percent of GSA:4 mol% Sm^{3+} nanophosphors

Element	Series	Atomic (%)	Weight (%)
Strontium (Sr)	L-series	18.51	4.51
Oxygen (O)	K-series	62.34	10.83
Aluminium (Al)	K-series	7.73	0.81
Gadolinium (Gd)	L-series	10.37	3.75
Samarium (Sm)	L-series	1.05	0.67

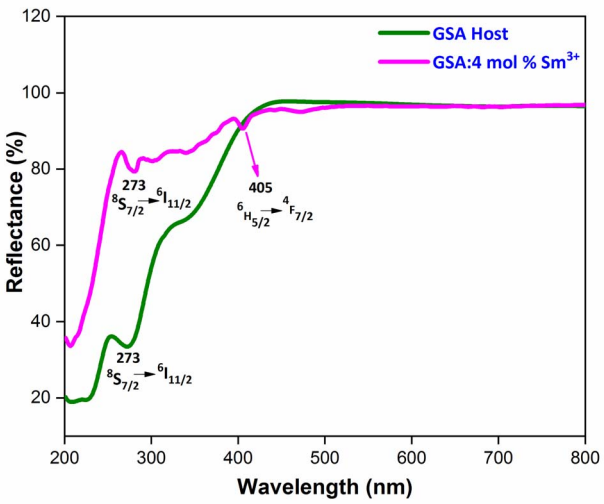

Fig. 8 Diffuse reflectance spectra of host $GdSr_2AlO_5$ and Sm^{3+} (4 mol%) doped $GdSr_2AlO_5$ phosphors.

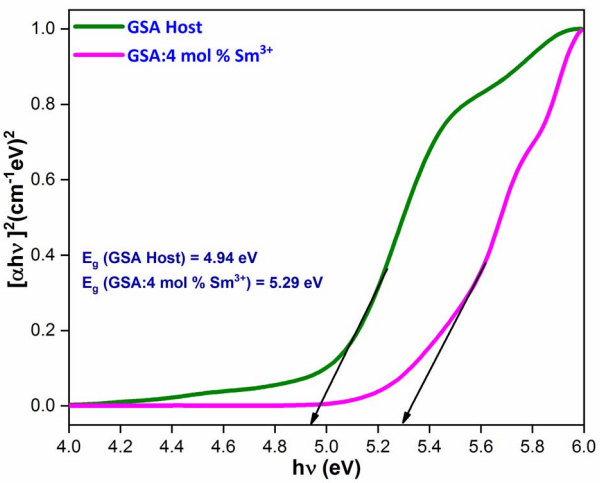

Fig. 9 for the $GdSr_2AlO_5$ and Sm^{3+} (4 mol%) doped $GdSr_2AlO_5$ phosphors.

3.2 TEM examination

TEM examination has been employed to comprehend dimensional features *i.e.* shape & size of crystalline materials. As we can see in Fig. 6, a non-uniform morphology has been observed comprising agglomerated nanoparticles in the range of 30–65 nanometers. The optical performance of the synthesized nanomaterials in the luminous field is supported by the findings of the diffraction probe and TEM examination, which closely resemble to one another.

3.3 EDX exploration

EDX spectrum analysis has shown that $Gd_{0.96}Sr_2AlO_5$:4 mol% Sm^{3+} nanophosphor were successfully fabricated. The dominating components in the manufactured nanosample might be identified owing to the spectral-lines in EDX shown in Fig. 7. Gd, Sr, Al, O, and Sm are the only spectral peaks in the EDX spectrum of the optimal sample, demonstrating that no other atoms are existing in the nanophosphor and that the desired material has produced with exact composition. The distinctive Sm^{3+} signal demonstrated that the former ion had been dispersed uniformly throughout the produced crystalline nanomaterial. EDX data (atomic & weight %) for $Gd_{0.96}Sr_2AlO_5$:4 mol% Sm^{3+} is shown in Table 5. The precise elemental distribution and stoichiometry of the homogenous nanophosphor composition are revealed by the EDX results.

3.4 Reflectance spectra and energy band gap analysis

To evaluate the optical characteristics and band gap of $GdSr_2AlO_5$ host and optimized $Gd_{0.96}Sr_2AlO_5$:4 mol% Sm^{3+} nanophosphors, reflectance spectra in the 200–800 nm wavelength range were measured, as displayed in Fig. 8. This graph unequivocally shows that the trivalent samarium ions distinctive peaks are associated to the DRS spectrum. Band gap of derived phosphor may be determined using Kubelka–Munk function (eqn (4)), which is defined as.[43]

$$F(R) = \frac{K}{S} = \frac{(1-R)^2}{2R} \quad (4)$$

here, R, S and K stand for reflectance, scattering coefficient and absorption coefficient correspondingly. However, Tauc's formulation (eqn (5)) provides the optical band gap (Eg) values.[44]

$$[F(R)h\nu]^2 = C_2(h\nu - E_g) \quad (5)$$

Upon extrapolation, $[F(R)h\nu]^2$ to 0 offset, the acquired E_g values are 4.94 & 5.29 eV for host and optimal doped nanophosphor, separately (Fig. 9). Optical band-gap values found to be increased with addition of Sm^{3+} ion content in host material, which was defined *via* Burstein–Moss effect.

3.5 Photoluminescence analysis

3.5.1 PL investigation of undoped $GdSr_2AlO_5$. The excitation and emission spectra of undoped $GdSr_2AlO_5$ crystalline nanomaterial synthesized *via* gel-combustion method is shown in Fig. 10(a and b) respectively. Fig. 10(a) demonstrates the PLE spectrum of $GdSr_2AlO_5$ in the spectral region of 200–300 nm which obtained by monitoring the emission wavelength at 324 nm. The major excitation peak at 276 nm is ascribed to the $^8S_{7/2} \rightarrow {}^6I_{11/2}$ transition of Gd^{3+} and minor peaks at 246 nm and 311 nm correspond to the $^8S_{7/2} \rightarrow {}^6D_{7/2}$ and $^8S_{7/2} \rightarrow {}^6P_{7/2}$ transition of Gd^{3+} ion.[45] Fig. 10(b) displays the emission spectrum of $GdSr_2AlO_5$ under 276 nm excitation. The sharp peak at 324 nm was observed due to the $^6P_J \rightarrow {}^8S_{7/2}$ transition of Gd^{3+} ion.[46]

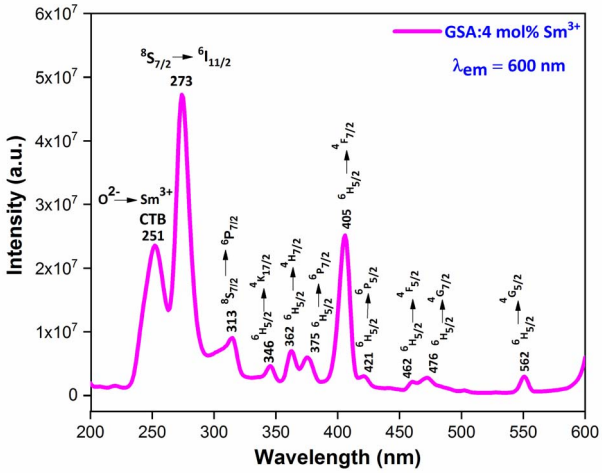

Fig. 11 PL excitation spectra of Sm^{3+} (4 mol%) doped $GdSr_2AlO_5$ phosphors.

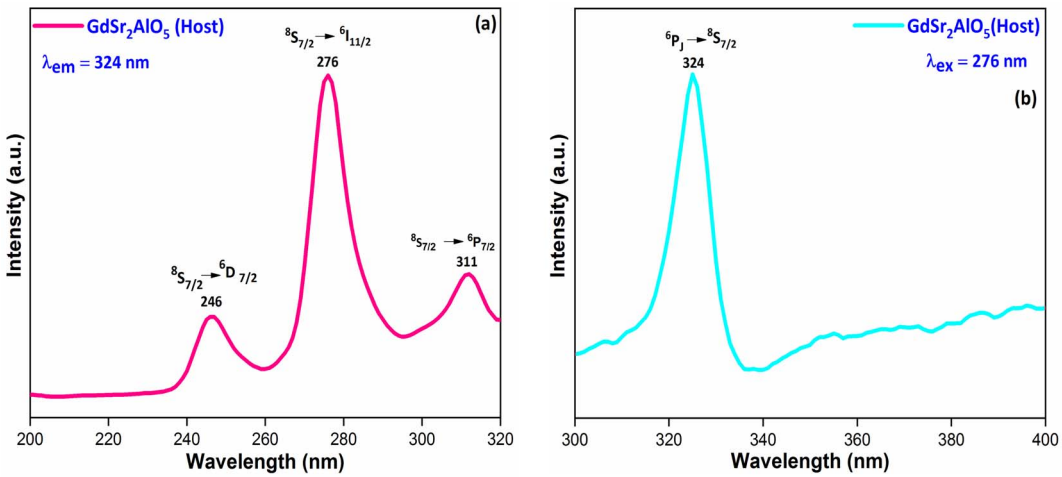

Fig. 10 Photoluminescence behaviour (a) excitation spectrum and (b) emission spectrum of host $GdSr_2AlO_5$ nanomaterial.

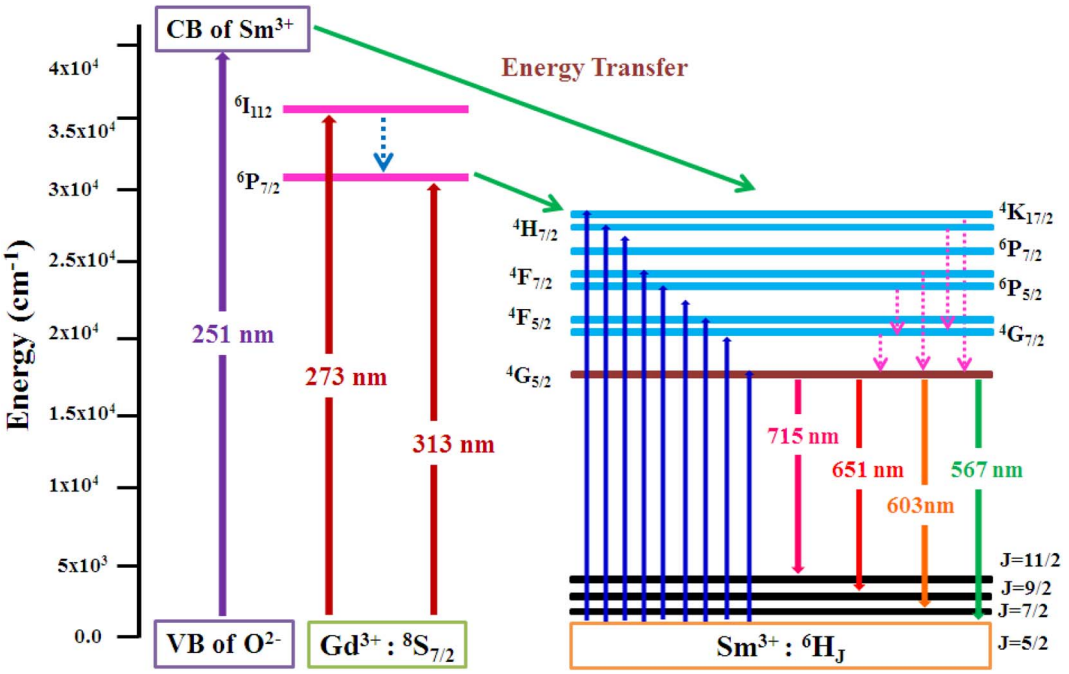

Fig. 12 Pictorial representation of energy transfer in the synthesized nanophosphors.

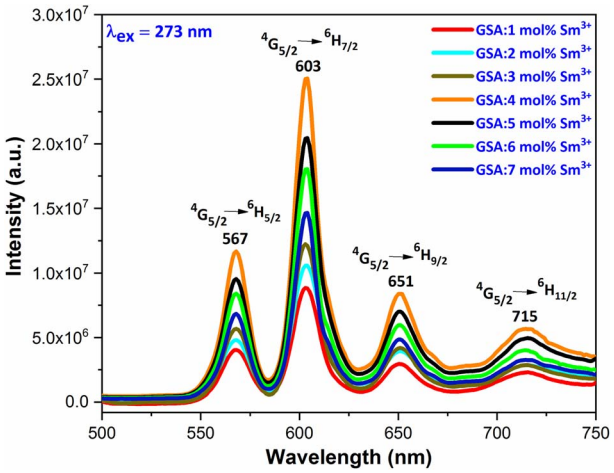

Fig. 13 Emission spectra of $Gd_{1-x}Sr_2AlO_5$:xSm^{3+} (x = 1–7 mol% Sm^{3+}) phosphors.

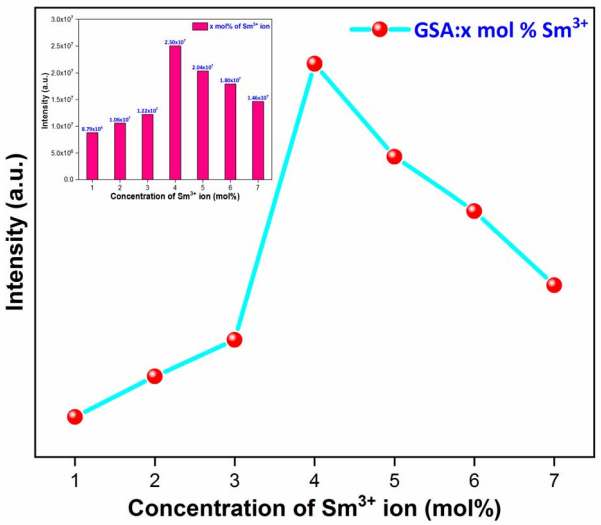

Fig. 14 Relative PL intensity of $Gd_{1-x}Sr_2AlO_5$:xSm^{3+} (x = 1–7 mol% Sm^{3+}) phosphors and inset represent the intensity of respective samples.

3.5.2 PLE investigation Sm^{3+} doped $GdSr_2AlO_5$. The PLE spectrum is examined at ~600 nm emission-wavelength of Sm^{3+} ion, represented in Fig. 11. There are numerous peaks perceived in the range 200–600 nm due to host ion and dopant ion. In PLE spectrum, charge transfer band (CTB) at 251 nm (O^{2-}–Sm^{3+}) and peaks due to the host ion are observed at 273 nm and 313 nm with $^8S_{7/2} \rightarrow {}^6I_{11/2}$ and $^6P_{7/2}$ separately.[47] While peaks perceived at 346 nm, 362 nm, 375 nm, 405 nm, 421 nm, 462 nm, 476 nm and 562 nm with transitions: $^6H_{5/2} \rightarrow {}^4K_{7/2}$, $^4H_{7/2}$, $^6P_{7/2}$, $^4F_{7/2}$, $^6P_{5/2}$, $^4G_{9/2}$, $^4F_{5/2}$, $^4G_{7/2}$ and $^4G_{5/2}$ correspondingly are due to intra f–f transitions of trivalent samarium ions.[48] The strongest band at ~273 nm is substantially intense than the other peaks detected owing to samarium ion, demonstrating that there is proficient energy-transfer takes place from Gd^{3+} to Sm^{3+} ion, displayed in Fig. 12.

3.5.3 PL investigation Sm^{3+} doped $GdSr_2AlO_5$. At an excitation wavelength of 273 nm, emission spectra in the range of 500–750 nm are captured for $Gd_{1-x}Sr_2AlO_5$:xSm^{3+} (x = 1–7 mol%) phosphors, as pictured in Fig. 13. The transition of the excited state $^4G_{5/2}$ of the Sm^{3+} ion to its ground states $^6H_{5/2}$, $^6H_{7/2}$, $^6H_{9/2}$, and $^6H_{11/2}$ is responsible for the narrow peaks at 567 nm (yellowish), 603 nm (orangish-red), 651 nm (red) and

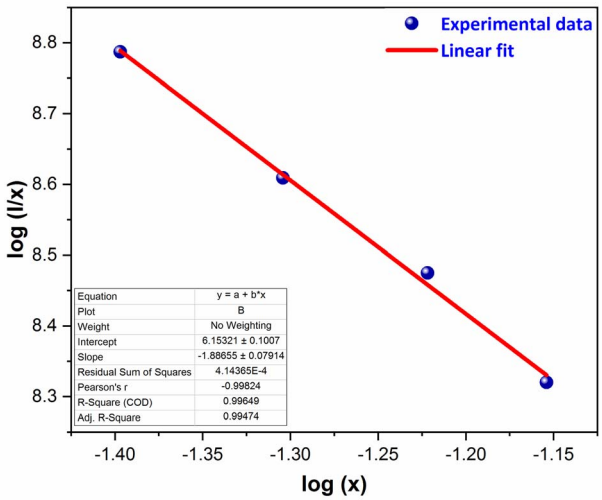

Fig. 15 Straight-line fitting of log(*I*/*x*) *vs.* log(*x*).

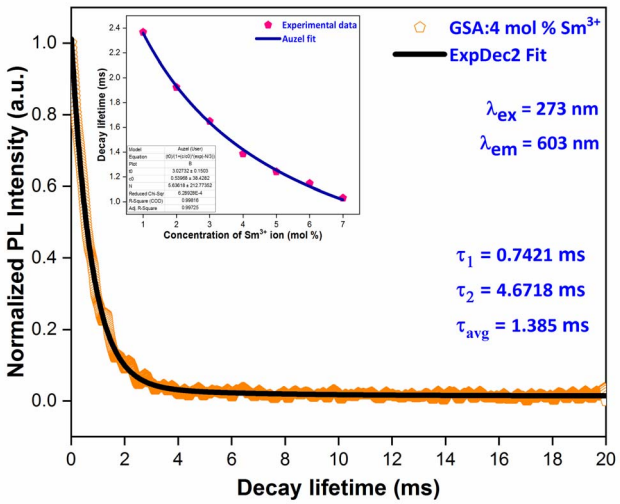

Fig. 16 PL decay curve $Gd_{0.96}Sr_2AlO_5$:4 mol% Sm^{3+} phosphors and inset represent the Auzel's fitting profile of all samples.

Table 6 Lifetime and quantum efficiency of GSA:xSm^{3+} ($x = 1$–7 mol% Sm^{3+}) phosphors

Sample	Decay-lifetime (ms)	Quantum-efficiency (η%)
GSA:1 mol% Sm^{3+}	2.367	78.19
GSA:2 mol% Sm^{3+}	1.924	63.56
GSA:3 mol% Sm^{3+}	1.624	54.47
GSA:4 mol% Sm^{3+}	1.385	45.75
GSA:5 mol% Sm^{3+}	1.241	40.99
GSA:6 mol% Sm^{3+}	1.147	37.89
GSA:7 mol% Sm^{3+}	1.031	34.07

715 nm (deep-red), separately.[49] The most dominant peak at 603 nm in all transitions of Sm^{3+} (1–7 mol%) doped $GdSr_2AlO_5$ phosphors corresponds to transition $^4G_{5/2} \rightarrow {}^6H_{7/2}$ of Sm^{3+} ion, which gives fabricated nanophosphors their orangish-red color. The quality of the Sm^{3+} ions transition $^4G_{5/2} \rightarrow {}^6H_{7/2}$ ($\Delta J = \pm 1$) positioned at 603 nm, is partly electric-dipole (ED) and partly magnetic dipole (MD). The transition $^4G_{5/2} \rightarrow {}^6H_{5/2}$ ($\Delta J = 0$), which is entirely MD in quality, is credited with producing the peak at 567 nm. Electronic transition $^4G_{5/2} \rightarrow {}^6H_{9/2}$ ($\Delta J = \pm 2$) is considered to be completely ED and is responsible for the peak at 651 nm. Nature forbids of the peak at 715 nm, which corresponds to $^4G_{5/2} \rightarrow {}^6H_{11/2}$ ($\Delta J = \pm 3$).[50] The local environment of the host matrix is extremely sensitive towards the ED transition. The Sm^{3+} ion occupies both symmetric and antisymmetric sites in the host lattice when the spectrum exhibits both the MD and ED transitions. The symmetry of Sm^{3+} ions in the coordination environment was assessed using the emission asymmetry ratio $R = I(^4G_{5/2} \rightarrow {}^6H_{9/2})/I(^4G_{5/2} \rightarrow {}^6H_{5/2})$ to explore the symmetry of the local environment.[51] It was widely known that the Sm^{3+} ions would present at low-symmetric locations if the ED transition was higher than the MD transition. The integrated-intensity of ED is lesser than the MD-transition, as seen in Fig. 12. Therefore, the dopant Sm^{3+} ions occupied the higher symmetry positions with inversion centre in the $GdSr_2AlO_5$ crystal structure, as demonstrated by the *R* value which computed to be lower than one.

3.5.4 Concentration quenching mechanism. When a dopant concentration is high, the distance between them shortens, causing increased non-radiative energy loss and a steady fall in luminescence intensity. This is known as the concentration quenching phenomena. Under 273 nm excitation, the emission spectra of Sm^{3+}-doped $GdSr_2AlO_5$ phosphors were perceived for a variation of Sm^{3+} concentrations (1–7 mol%), a comparable representation is shown in Fig. 14. Emission strength increases by up to 4 mol% as the Sm^{3+} ion concentration increases. Additionally, it drops for a small proportion due to the concentration quenching function. The historical profile (inset of Fig. 14) presents the intensity of the all synthesized samples. Thus, 4 mol percent is thought to be the optimal Sm^{3+} ion concentration. The non-radiative energy transfer process takes place when the distance between neighbouring Sm^{3+} ions is so short that only making contact with one another will cause this effect. According to Blasse's calculations, the increase in dopant ions density permits the distance between them to close, which may be advantageous for non radiative straits by promoting interchange of electrons (e^-) between incoming ions rather than radiative-emanations. Concentration quenching refers to the slowing down of emission caused by non-radiative stimulation at high activator-ion concentrations. Remarkably, the critical distance *i.e.* R_C between the nearby ions value is roughly measured *via* applying the following relation (eqn (6)).[52]

$$R_C = 2\left(\frac{3V}{4\pi x_C Z}\right)^{1/3} \quad (6)$$

here *V*, x_c & *Z* signifies the volume of the unit cell, optimized dopant concentration and the number of cationic sites offered for the dopant ions per unit cell, individually. For optimum sample, $V = 525.948$, $Z = 4$, and $x_c = 0.04$, R_c was 18.45 Å which

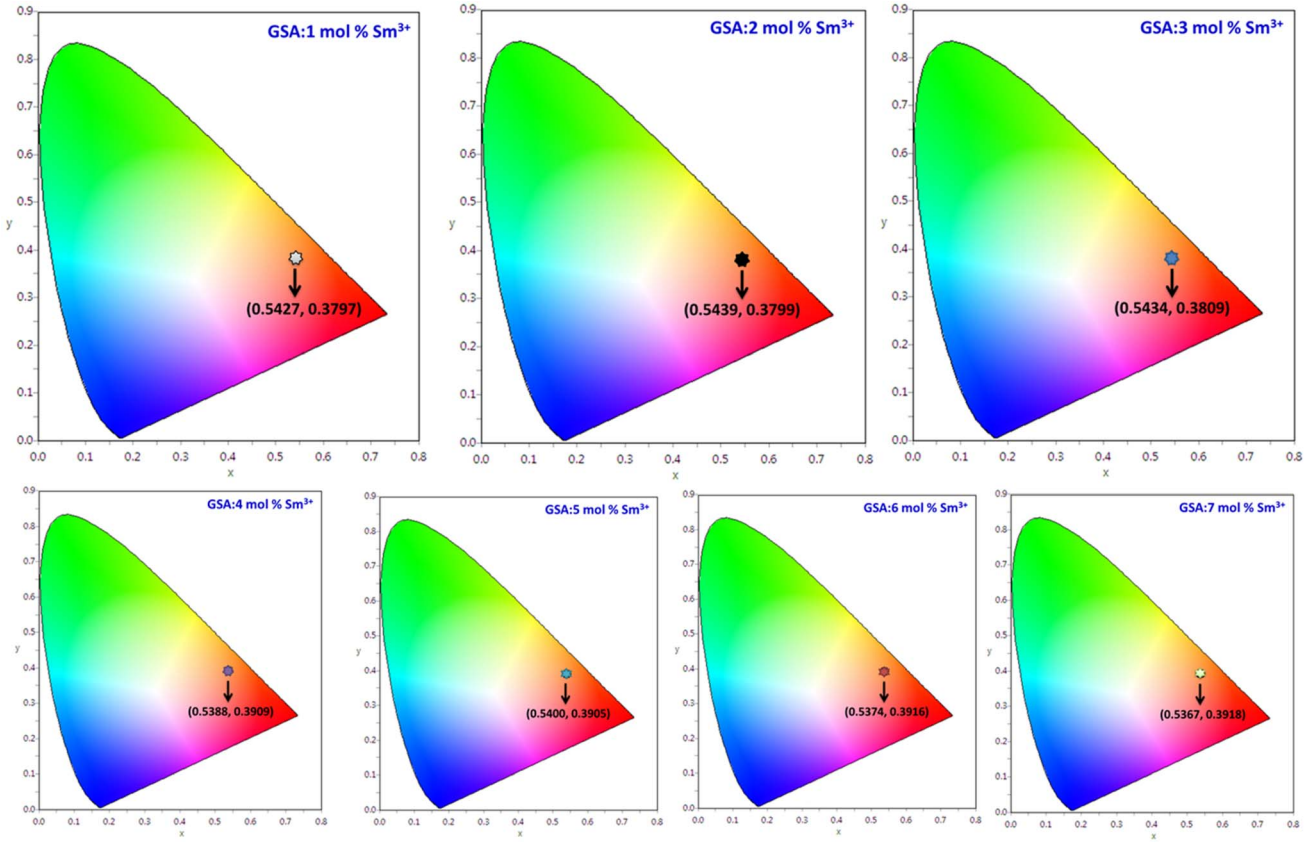

Fig. 17 CIE coordinates of $Gd_{1-x}Sr_2AlO_5$:*x* mol% Sm^{3+} (1–7 mol%) phosphors.

was greater than 5 Å. Elimination luminous effect can only be explained by multipolar interface since there is no convergence between the PLE and PL spectra in present context and the critical-gap is more than 5. To further authenticate the mechanism of energy transfer in $Gd_{0.96}Sr_2AlO_5$:4 mol% Sm^{3+} nanophosphors, Dexter's formula is used (eqn (7))[53]

$$\log\left(\frac{I}{x}\right) = k - \frac{M}{3}\log(x) \quad (7)$$

here, I signify the PL intensity at dopant concentration x, K and β are constants & M is the interactions type. M denotes the concentration quenching, which includes three different mechanisms: dipole–dipole, dipole-quadrupole, and quadrupole–quadrupole. These three mechanisms correspond to the values of $M = 6$, 8, and 10.[54] According to Fig. 15, which shows a straight-line connection between $\log(I/x)$ and $\log(x)$ with a slope value of −1.886, and M value determined to be 5.658 (nearby to 6). The calculated value suggested that the primary mechanism of energy transfer in $GdSr_2AlO_5$:Sm^{3+} nanophosphors are dipolar–dipolar (d–d) interaction.

3.6 Luminescence decay time

Fig. 16 displays the PL decay curve of $Gd_{0.96}Sr_2AlO_5$:4 mol% Sm^{3+} powdered nanocrystalline material under excitation (Ex) and emission (Em) wavelengths of 273 and 603 nm. The Sm^{3+} ions are initially stimulated to higher excited states while monitored with excitation wavelength of 273 nm, and then subsequently relaxed to the ground state *via* relaxation or non-radiative energy transfer. The lifetime-curve is perfectly fitted through Bi-exponential approach followed by the eqn (8) (ref. 55)

$$I_t = I_0 + A_1\exp(-t/\tau_1) + A_2\exp(-t/\tau_2) \quad (8)$$

Among them, I_t correspond to the emission intensity at time $= t$, I_0 is initial emission intensity, τ_1 and τ_2 refers to the decay lifetimes and A_1 & A_2 are their fitting constants. Average decay time (τ_{avg}) of Sm^{3+} ions can be determined by using following expression (eqn (9)).[56]

$$\tau_{avg} = (A_1t_1^2 + A_2t_2^2)/(A_1t_1 + A_2t_2) \quad (9)$$

In Table 6, the average lifespan values (avg) for all doped nanosamples are displayed. We can see that decay times diminish as Sm^{3+} ion doping level raises. The ions originate near to one another and rapidly transfer energy as the content of activator ions rises, resulting in a new decay route with shorter decay duration. Inset of Fig. 16 proves that the Auzel's fitting (eqn (10)) way results in a τ_c value of 3.027 ms.[57]

$$\tau_C = \tau_0/1 + \frac{C}{C_0}e^{-N/3} \quad (10)$$

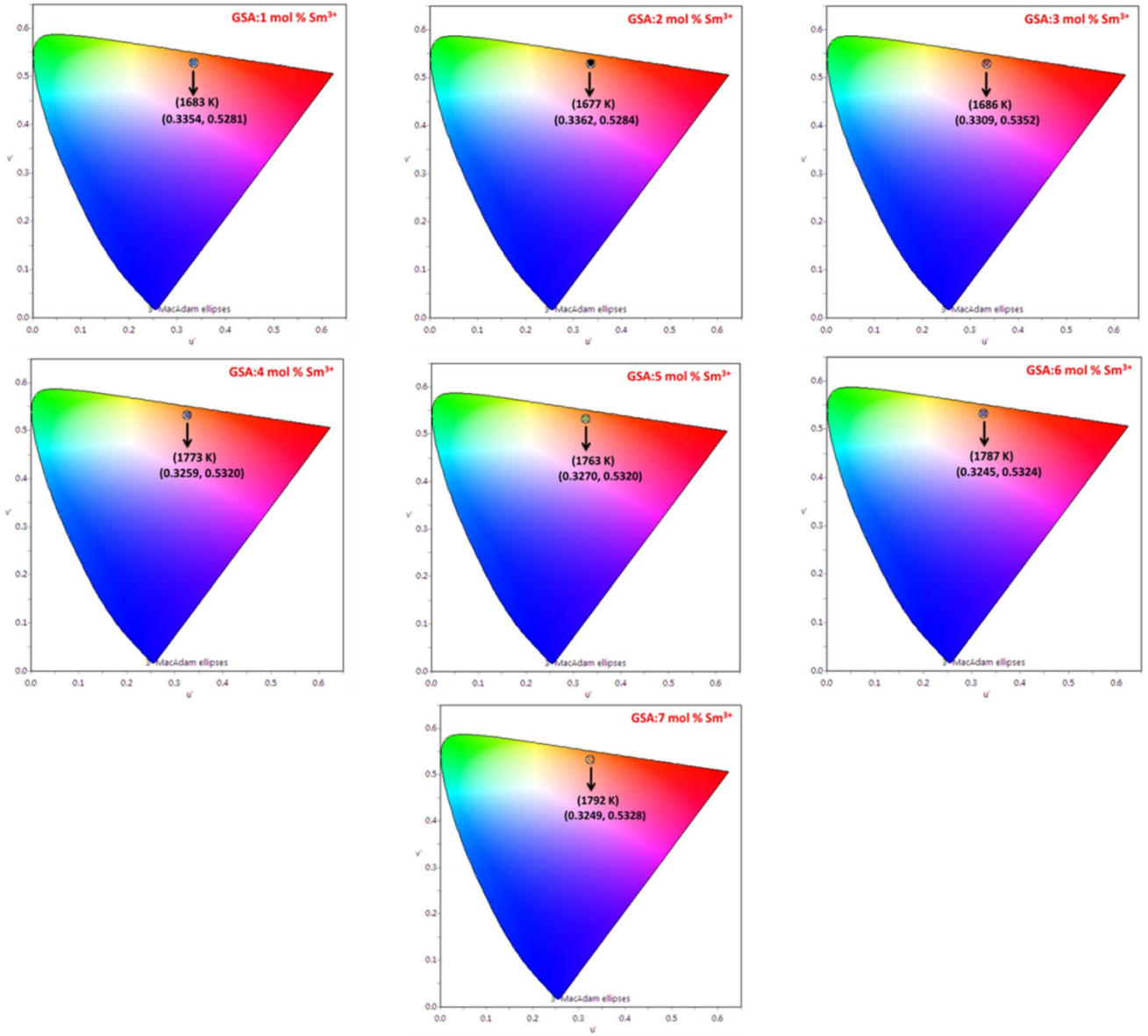

Fig. 18 Representation of u', v' with CCT values of $Gd_{1-x}Sr_2AlO_5$:x mol% Sm^{3+} (1–7 mol%) phosphors.

Table 7 Chromaticity parameters of $Gd_{1-x}Sr_2AlO_5$:xSm^{3+} (x = 1–7 mol% Sm^{3+}) nanophosphors

Sample	(x, y)	CP (%)	(u', v')	CCT (K)
GSA:1 mol% Sm^{3+}	0.5427, 0.3797	79.81	0.3354, 0.5281	1683
GSA:2 mol% Sm^{3+}	0.5439, 0.3799	81.22	0.3362, 0.5284	1677
GSA:3 mol% Sm^{3+}	0.5434, 0.3809	82.04	0.3309, 0.5352	1686
GSA:4 mol% Sm^{3+}	0.5388, 0.3909	87.55	0.3259, 0.5320	1773
GSA:5 mol% Sm^{3+}	0.5400, 0.3905	86.27	0.3270, 0.5320	1763
GSA:6 mol% Sm^{3+}	0.5374, 0.3916	82.03	0.3245, 0.5324	1787
GSA:7 mol% Sm^{3+}	0.5367, 0.3918	81.75	0.3249, 0.5328	1792

here, τ_C = decay-time, C_0 = constant and N tells about the phonon number. Also, quantum-efficiency (η) of activated nanomaterials is assessed by the help of formulation given below (eqn (11))[58]

$$\eta = \tau_{avg}/\tau_0 \quad (11)$$

The obtained quantum efficiency (η) values of synthesized nanophosphors are listed in Table 6, which shows that η values are gradually declined with rise in the doping level of Sm^{3+} ions owed to the proportionate rise in the rate of radiation less energy transfer. The measured quantum efficiency is obtained within suitable range in the present case, suggesting that the processed phosphors are beneficial for LED applications.

3.7 Colorimetric investigation

To verify the color of the emitting visible radiation, CIE diagrams and coordinates were employed. Using Commission Internationale de I'Eclairage (CIE) 1931 standards, the samples

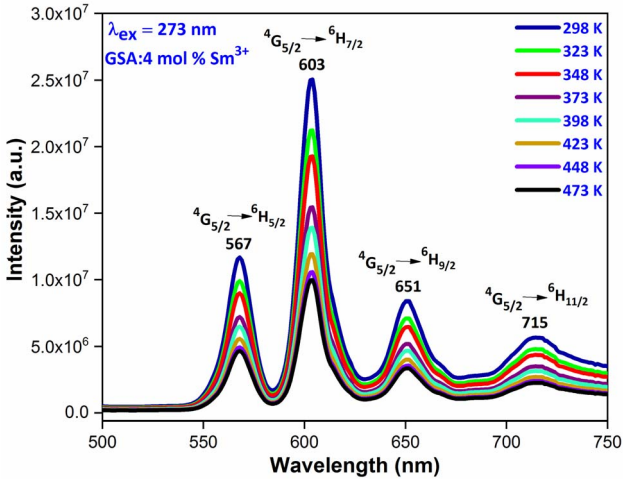

Fig. 19 Temperature dependent emission spectra of GSA: 4 mol% Sm^{3+} nanophosphor in the temperature range of 298–473 K.

CIE chromaticity values were key technical characteristics in the CIE 1931 chromaticity diagram. The $Gd_{1-x}Sr_2AlO_5:xSm^{3+}$ (x = 1–7 mol%) phosphors chromaticity coordinates, as seen in Fig. 17, are placed near the reddish-orange color area, which marks the edge of the CIE 1931 chromaticity chart. Furthermore, while dealing with thin band emanation spectrums, the measurement of color purity (CP) is important. In this instance, we were able to observe the narrow band emission in the orange-reddish province at 603 nm. Therefore, using the following eqn (12), we assess the CP % of generated nanomaterials that produce orange–red color.[59]

$$CP = \sqrt{\frac{(x - x_i)^2 + (y - y_i)^2}{(x_d - x_i)^2 + (y_d - y_i)^2}} \times 100 \quad (12)$$

Here, (x, y) are CIE points, (x_i, y_i) are illuminate points and (x_d, y_d) are the dominating color-coordinates. The observed average CP value is 82.18%. Furthermore, because of CIE-points being at border of the CIE-chart, the CP value of 4 mol% activated powder is maximal (87.55%). When combined with other phosphor powders, the color characteristics of the generated powders show that these phosphors may be employed successfully in orange-reddish emanating devices and as prospective applicant in fabrication of wLEDs. One crucial luminous characteristic used to assess the performance of the phosphors is CCT. Typically, lights are regarded as producing warm light when their CCT was lower than 3000 K. The lights were classified as cool light even though their CCT was more than 4000 K. The McCamy empirical formulation (eqn (13)) served as a means of expressing the values of CCT.[60]

$$CCT = -437n^3 + 3601n^2 - 6861n + 5514.31 \quad (13)$$

where, $n = (x - x_e)/(y - y_e)$, (x, y) are product's chromaticity coordinates and (x_e, y_e) is the epicenter position with $x_e = 0.332$ and $y_e = 0.186$. The variation of CIE-point (x, y to u', v') to evaluate CCT values encompasses following calculations (eqn (14)).[61]

$$u' = \frac{4x}{-2x + 12y + 3} \quad v' = \frac{9y}{-2x + 12y + 3} \quad (14)$$

The $Gd_{1-x}Sr_2AlO_5:xSm^{3+}$ (x = 1–7 mol%) phosphor's u', v' along with their CCT values, are seen in Fig. 18. Table 7 lists all the CCT values along with their corresponding u', v', color purity and CIE color coordinates. It was also observed that the CCTs varied within a color space, with a minimum value of 1683 K and a high value of 1792 K. The low CCTs demonstrated that warm light LEDs have a promising future for using the phosphors in their as-prepared state.

3.8 Thermal stability behavior

Thermal stability is closely related to the application of the nanophosphors. In order to explore the thermal stability of materials, the temperature-dependent emission spectra of $Gd_{0.96}Sr_2AlO_5$:4 mol% Sm^{3+} were measured in the temperature range of 298–473 K with the interval of 25 K, as shown in Fig. 19. It is beneficial to have a comprehensive understanding of the thermal deterioration of the phosphors so as to improve their performance *via* material design. These emission spectra present almost same spectral distribution *i.e.* the shape and position of the observed peaks are almost similar, suggesting that this phosphor has excellent color stability. With the temperature increase, the emission intensities decrease gradually due to the well-known thermal quenching effect.[62,63] Generally, with the increase of temperature, the probabilities of multiphonon relaxation and energy transfer for quenching the emitting levels may be enhanced, which are responsible for the decrease of luminescence intensity

4 Conclusions

The extensive effort made to produce white light-emitting diodes (wLEDs), which have the ability to provide with enhanced photoluminescence (PL) capabilities, is an indication of modernity. The orange phosphor, one of the crucial elements needed for the mass manufacture of warm wLEDs. This research makes an effort to synthesize a series of $Gd_{1-x}Sr_2AlO_5:xSm^{3+}$ (x = 1–7 mol%) phosphor *via* combustion route to address this problem.

The produced phosphors are in a single phase, according to XRD measurements. It found to be a pure tetragonal crystal structure with *I*4/*mcm* (140) space group symmetry. The $^4G_{5/2} \rightarrow {}^6H_{7/2}$ transition of Sm^{3+} ions which was exhibited by the synthesized phosphors excited at 273 nm is responsible for the vivid orange–red emission at 603 nm. The dipole–dipole (d–d) interaction is the major reason for the concentration quenching process, as determined by calculations ($R_c = 18.45$ and $Q = 6$) and investigation. According to calculations, the prepared crystalline nanophosphors having decay lifetimes ranged from 2.367 ms to 1.031 ms. The colorimetric examination *i.e.* chromaticity coordinates (CIE), low CCTs values and high color purity (CP) endorses their potential usages in the fabrication of warm wLEDs.

5 Credit author statement

Pawan Kumar: Data curation, writing – original draft, investigation, methodology, software; Devender Singh: Writing – review & editing, resources, supervision; Isha Gupta: visualization, validation.

Conflicts of interest

The authors declare that they have no known competing financial interests or personal relationships that could have appeared to influence the work reported in this paper.

Data availability

Data will be made available on request

Acknowledgements

The author (Pawan Kumar) is thankful to UGC-New Delhi for providing JRF [117/(CSIRNETJUNE2019)].

References

1 Q. M. Le, T. H. Tran, T. H. Nguyen, T. K. Hoang, T. B. Nguyen, K. T. Do and N. A. T. Nguyen, Development of a fluorescent label tool based on lanthanide nanophosphors for viral biomedical application, *Adv. Nat. Sci.: Nanosci. Nanotechnol.*, 2012, **3**, 035003.

2 A. Bergh, G. Craford, A. Duggal and R. Haitz, The promise and challenge of solid-state lighting, *Phys. Today*, 2001, **54**, 42–47.

3 I. Gupta, S. Singh, S. Bhagwan and D. Singh, Rare earth (RE) doped phosphors and their emerging applications: A review, *Ceram. Int.*, 2021, **47**, 19282–19303.

4 X. Li, W. Cai, H. Guan, S. Zhao, S. Cao, C. Chen and Z. Zang, Highly stable $CsPbBr_3$ quantum dots by silica-coating and ligand modification for white light-emitting diodes and visible light communication, *J. Chem. Eng.*, 2021, **419**, 129551.

5 H. Guan, S. Zhao, H. Wang, D. Yan, M. Wang and Z. Zang, Room temperature synthesis of stable single silica-coated $CsPbBr_3$ quantum dots combining tunable red emission of Ag–In–Zn–S for High-CRI white light-emitting diodes, *Nano Energy*, 2020, **67**, 104279.

6 S. Itoh, M. Tanaka and T. Tonegawa, Development of field emission displays, *J. Vac. Sci. Technol., B: Nanotechnol. Microelectron.: Mater., Process., Meas., Phenom.*, 2004, **22**, 1362–1366.

7 P. Kumar, D. Singh, I. Gupta, S. Singh and V. Kumar, Structural and luminescent characteristics of orthorhombic $GdAlO_3:Sm^{3+}$ nanocrystalline materials for solid state lighting, *Chem. Phys. Lett.*, 2022, **812**, 140277.

8 X. Li, W. Ma, D. Liang, W. Cai, S. Zhao and Z. Zang, High-performance $CsPbBr_3$@ Cs_4PbBr_6/SiO_2 nanocrystals via double coating layers for white light emission and visible light communication, *eScience*, 2022, **6**, 646–654.

9 R. Wang, H. Xiang, J. Chen, Y. Li, Y. Zhou, W. C. Choy, Z. Fan and H. Zeng, Energy regulation in White-Light-Emitting Diodes, *ACS Energy Lett.*, 2022, **7**, 2173–2188.

10 P. Kumar, S. Singh, I. Gupta, V. Kumar and D. Singh, Preparation and luminescence behaviour of perovskite $LaAlO_3:Tb^{3+}$ nanophosphors for innovative displays, *Optik*, 2022, **267**, 169709.

11 D. Yan, S. Zhao, Y. Zhang, H. Wang and Z. Zang, Highly efficient emission and high-CRI warm white light-emitting diodes from ligand-modified $CsPbBr_3$ quantum dots, *Opto-Electron. Adv.*, 2022, **5**, 200075.

12 R. Sharma, R. Laishram, B. K. Gupta, R. Srivastva and O. P. Sinha, A review on MX_2 (M= Mo, W and X= S, Se) layered material for opto-electronic devices, *Adv. Nat. Sci.: Nanosci. Nanotechnol.*, 2022, **13**, 023001.

13 I. Gupta, S. Singh, P. Kumar, S. Bhagwan, V. Kumar and D. Singh, Structural, morphological and optoelectronic aspects of $YAlO_3:Dy^{3+}$ doped nanocrystalline materials for NUV energized WLEDs, *Curr. Appl. Phys.*, 2022, **42**, 78–89.

14 B. Karthikeyan and R. Vettumperumal, Optical and electrochemical properties of pure and Ti-doped CdO nanoparticles for device applications, *Mater. Sci. Eng., B*, 2022, **281**, 115754.

15 L. Zhao, P. Xu, F. Fan, J. Yu, Y. Shang, Y. Li, L. Huang and R. Yu, Synthesis and photoluminescence properties of Sm^{3+} and Dy^{3+} ions activated double perovskite Sr_2MgTeO_6 phosphors, *J. Lumin.*, 2019, **207**, 520–525.

16 I. Gupta, D. Singh, S. Singh, P. Kumar, S. Bhagwan and V. Kumar, Structural and photophysical measurements of Er^{3+} doped $Gd_4Al_2O_9$ nanophosphors for NUV excitable solid-state lighting applications, *Chem. Phys. Lett.*, 2023, **814**, 140350.

17 D. N. Chung, D. N. Hieu, T. T. Thao, V. V. Truong and N. N. Dinh, Synthesis and characterization of Ce-doped $Y_3Al_5O_{12}$ (YAG:Ce) nanopowders used for solid-state lighting, *J. Nanomater.*, 2014, **2014**, 1–7.

18 C. Liu, S. Pokhrel, C. Tessarek, H. Li, M. Schowalter, A. Rosenauer and L. Mädler, Rare-earth-doped $Y_4Al_2O_9$ nanoparticles for stable light-converting phosphors, *ACS Appl. Nano Mater.*, 2019, **3**, 699–710.

19 S. R. Anishia, M. T. Jose, O. Annalakshmi and V. Ramasamy, Thermoluminescence properties of rare earth doped lithium magnesium borate phosphors, *J. Lumin.*, 2011, **131**, 2492–2498.

20 I. Gupta, D. Singh, S. Singh, P. Kumar, S. Bhagwan and V. Kumar, Phase recognition and spectroscopic characteristics of single-phase Tb^{3+} doped $Gd_4Al_2O_9$ nanophosphors for NUV energized advanced photonic appliances, *J. Lumin.*, 2022, **252**, 119327.

21 Q. Mo, C. Chen, W. Cai, S. Zhao, D. Yan and Z. Zang, Room temperature synthesis of stable zirconia-coated $CsPbBr_3$ nanocrystals for white light-emitting diodes and visible light communication, *Laser Photonics Rev.*, 2021, **15**, 2100278.

22 V. Tanwar, S. Singh, I. Gupta, P. Kumar, H. Kumar, B. Mari and D. Singh, Preparation and luminescence characterization of Eu (III)-activated Forsterite for

optoelectronic applications, *J. Mol. Struct.*, 2022, **1250**, 131802.

23 A. Varma, A. S. Mukasyan, A. S. Rogachev and K. V. Manukyan, Solution combustion synthesis of nanoscale materials, *Chem. Rev.*, 2016, **116**, 14493–14586.

24 P. Kumar, D. Singh, I. Gupta, S. Singh, V. Kumar, H. Kumar and S. K. Chhikara, Perovskite $GdAlO_3$:Dy^{3+} nanophosphors: A gel-combustion synthesis, phase evaluation and down conversion luminescent characteristics for lighting applications, *J. Lumin.*, 2022, **252**, 119409.

25 G. Zhang, Q. Qiang, S. Du and Y. Wang, An upconversion luminescence and temperature sensor based on Yb^{3+}/Er^{3+} co-doped $GdSr_2AlO_5$, *RSC Adv.*, 2018, **8**, 9512–9518.

26 W. T. Hong and H. K. Yang, Luminescence Properties of a Yellow $GdSr_2AlO_5$:Ce^{3+} Phosphor for a White LED, *New Phys.*, 2015, **65**, 1181–1186.

27 I. Gupta, P. Kumar, S. Singh, S. Bhagwan, V. Kumar and D. Singh, Phase recognition, structural measurements and photoluminescence studies of reddish-orange-emissive $YAlO_3$:Sm^{3+} perovskite nanophosphors for NUV energized WLEDs, *J. Mol. Struct.*, 2022, **1267**, 133567.

28 R. Amari, E. Benrezgua, B. Deghfel, Z. Abdelhalim, M. K. Yaakob, W. J. Basirun, A. Boukhari, S. Kheawhom and A. A. Mohamad, Ni doping effect on the electronic, structural and optical properties of ZnO nanoparticles prepared by Co-precipitation route, *Opt. Mater.*, 2022, **128**, 112398.

29 S. Singh and D. Singh, Down-conversion and structural characterizations of trivalent terbium- doped garnet nanocrystalline phosphors for lighting applications, *J. Mater. Sci.: Mater. Electron.*, 2021, **32**, 17674–17685.

30 I. Gupta, P. Kumar, S. Singh, S. Bhagwan, S. K. Chhikara and D. Singh, Crystal configuration, spectroscopic and optical characteristics of Er^{3+} doped $YAlO_3$ perovskites for advanced photonic appliances, *Inorg. Chim. Acta*, 2022, **543**, 121183.

31 S. Tajik and H. Beitollahi, Hydrothermal synthesis of $CuFe_2O_4$ nanoparticles for highly sensitive electrochemical detection of sunset yellow, *Food Chem. Toxicol.*, 2022, **165**, 113048.

32 A. Li, Z. Li, L. Pan, Z. Wang, W. Chen, Q. Shao and Y. Tang, Upconversion luminescent nanoheater based on $NaGd(MoO_4)_2$:Yb^{3+}/Tm^{3+} nanocrystals: Surfactant-free solvothermal synthesis, upconversion photoluminescence and photothermal conversion, *J. Alloys Compd.*, 2022, **904**, 164087.

33 P. Kumar, D. Singh, I. Gupta, S. Singh and V. Kumar, Emerging green light emission of Er^{3+}-activated single phased $GdAlO_3$ phosphors for lighting applications, *Luminescence*, 2022, **37**, 2028–2040.

34 P. Kumar, S. Singh, I. Gupta, K. Nehra, V. Kumar and D. Singh, Structural refinement and optical characteristics of single-phase $Gd_3Al_5O_{12}$:Er^{3+} nanophosphors for luminescent applications, *J. Lumin.*, 2022, **252**, 119338.

35 D. Singh and S. Kadyan, Synthesis and optical characterization of trivalent europium doped $M_4Al_2O_9$ (M= Y, Gd and La) nanomaterials for display applications, *J. Mater. Sci.: Mater. Electron.*, 2017, **28**, 11142–11150.

36 G. Li, Y. Wang, W. Zeng, W. Chen, S. Han and H. Guo, Luminescent and magnetic properties of the afterglow phosphors $GdSr_2AlO_5$: RE^{3+} (RE^{3+}= Eu^{3+}, Sm^{3+}, Pr^{3+} and Dy^{3+}), *RSC Adv.*, 2015, **5**, 20884–20889.

37 P. Kumar, S. Singh, I. Gupta, V. Kumar and D. Singh, Luminous $LaAlO_3$:Dy^{3+} perovskite nanomaterials: Synthesis, structural and luminescent characteristics for WLEDs, *Luminescence*, 2022, **37**, 1932–1941.

38 G. U. Xiguang, F. U. Renli, W. Jiang, P. Zhang, T. A. N. G. Ye and A. CoŞGun, Photoluminescence properties of an orange-red $LaSr_2AlO_5$: Sm^{3+} phosphor prepared by the Pechini-type sol-gel process, *J. Rare Earths*, 2015, **33**, 954–960.

39 S. Singh, I. Gupta and D. Singh, Sm^{3+}-activated YAG nanocrystals: Synthesis, structural and spectroscopic analysis for orange-red emitting LEDs, *Optik*, 2021, **238**, 166482.

40 K. Li, H. Lian and R. V. Deuna, Site occupancy and photoluminescence properties of a novel deep-red-emitting phosphor $NaMgGdTeO_6$:Mn^{4+} with perovskite structure for w-LEDs, *J. Lumin.*, 2018, **198**, 155–162.

41 U. Holzwarth and N. Gibson, The Scherrer equation versus the 'Debye-Scherrer equation', *Nat. Nanotechnol.*, 2011, **6**, 534.

42 S. Bathula, B. Gahtori, M. Jayasimhadri, S. K. Tripathy, K. Tyagi, A. K. Srivastava and A. Dhar, Microstructure and mechanical properties of thermoelectric nanostructured n-type silicon-germanium alloys synthesized employing spark plasma sintering, *Appl. Phys. Lett.*, 2014, **105**, 061902–061904.

43 P. K. Jisha, S. C. Prashantha and H. Nagabhushana, Luminescent properties of Tb doped gadolinium aluminate nanophosphors for display and forensic applications, *J. Sci.: Adv. Mater. Devices*, 2017, **2**, 437–444.

44 P. Kumar, D. Singh, I. Gupta, S. Singh, S. Nehra and R. Kumar, Realization of warm reddish-orange light emitter single phase $Y_4Al_2O_9$: Sm^{3+} nanophosphors for indoor lighting applications, *J. Lumin.*, 2023, **257**, 119703.

45 P. K. Jisha, S. C. Prashantha and H. Nagabhushana, Luminescent properties of Tb doped gadolinium aluminate nanophosphors for display and forensic applications, *J. Sci.: Adv. Mater. Devices*, 2017, **2**, 437–444.

46 P. Gupta, A. K. Bedyal, V. Kumar, Y. Khajuria, V. Sharma, O. M. Ntwaeaborwa and H. C. Swart, Energy transfer mechanism from Gd^{3+} to Sm^{3+} in $K_3Gd(PO_4)_2$:Sm^{3+} phosphor, *Mater. Res. Express*, 2015, **2**, 076202.

47 P. Kumar, D. Singh, I. Gupta, S. Singh, V. Kumar, H. Kumar and S. K. Chhikara, Cool green light emitting $GdAlO_3$:Tb^{3+} perovskite nanomaterials: Crystal structure and spectroscopic characteristics for advance display appliances, *Inorg. Chem. Commun.*, 2022, **154**, 110064.

48 P. Kumar, S. Singh, I. Gupta, V. Kumar and D. Singh, Structural and optical characterization of trivalent samarium-activated $LaAlO_3$ nanocrystalline materials for solid-state lighting, *J. Mol. Struct.*, 2022, **1265**, 133362.

49 P. Kumar, S. Singh, I. Gupta, A. Hooda, V. Kumar and D. Singh, Reddish-orange color tunable Sm^{3+} activated $Gd_3Al_5O_{12}$ phosphors: Crystallographic and photophysical investigation for lighting applications, *J. Mol. Struct.*, 2022, **1271**, 134074.

50 R. B. Basavaraj, S. Kumar, D. P. Aarti, G. Nagaraju, H. S. Kumar, R. Soundar and M. Shahsank, Color tunable orange-red light emitting Sm^{3+} doped $BaZrO_3$ nanopowders: Photoluminescence properties for w-LED applications, *Inorg. Chem. Commun.*, 2021, **128**, 108577.

51 W. U. Khan, L. Zhou, X. Li, W. Zhou, D. Khan, S. I. Niaz and M. Wu, Single phase white LED phosphor $Ca_3YAl_3B_4O_{15}$: Ce^{3+}, Tb^{3+}, Sm^{3+} with superior performance: color-tunable and energy transfer study, *Chem. Eng. J.*, 2021, **410**, 128455.

52 G. Blasse, Energy transfer in oxidic phosphors, *Philips Res. Rep.*, 1969, **24**, 131–144.

53 I. Gupta, D. Singh, S. Singh, P. Kumar, S. Bhagwan and V. Kumar, Study of structural and spectroscopic characteristics of novel color tunable yellowish-white Dy^{3+} doped $Gd_4Al_2O_9$ nanophosphors for NUV-based WLEDs, *J. Mol. Struct.*, 2022, **1272**, 134199.

54 P. Kumar, S. Singh, I. Gupta, V. Kumar and D. Singh, Er^{3+}-activated $LaAlO_3$ perovskite phosphor: Crystal structure and down conversion photoluminescent behaviour for optoelectronic devices, *Inorg. Chem. Commun.*, 2022, **1265**, 109578.

55 P. Kumar, S. Singh, I. Gupta, A. Dalal, V. Kumar and D. Singh, Preparation, structural and photometric properties of single-phased $Gd_3Al_5O_{12}$:Tb^{3+} green-emitting phosphors for solid state lighting purpose, *Mater. Sci. Eng.*, 2023, **288**, 116189.

56 I. Gupta, S. Singh, P. Kumar, S. Bhagwan, V. Tanwar, S. Nehra and D. Singh, Synthetic, structural and optical characteristic of novel color tunable reddish-orange $Gd_4Al_2O_9$: Sm^{3+} nanocrystalline materials for solid-state photonic appliances, *Inorg. Chem. Commun. B.*, 2022, **148**, 110332.

57 P. Dang, G. Li, S. Liang, H. Lian and J. Lin, Multichannel photoluminescence tuning in Eu-doped apatite phosphors via coexisting cation substitution, energy transfer and valence mixing, *J. Mater. Chem. C*, 2019, **7**, 5975–5987.

58 P. Kumar, S. Singh, I. Gupta, K. Nehra, V. Kumar and D. Singh, Structural and luminescent behaviour of Dy(III) activated $Gd_3Al_5O_{12}$ nanophosphors for white-LEDs applications, *Mater. Chem. Phys.*, 2022, **295**, 127035.

59 K. Nehra, A. Dalal, A. Hooda, P. Kumar, D. Singh, S. Kumar, R. S. Malik and P. Kumar, Luminous terbium and samarium complexes with diacetylmethane and substituted 1,10-phenanthroline derivatives for display applications: Preparation and optoelectronic investigations, *J. Lumin.*, 2022, **249**, 119032.

60 A. Hooda, A. Dalal, K. Nehra, P. Kumar, D. Singh, S. Kumar, R. S. Malik, R. Kumar and P. Kumar, Mononuclear luminous β-diketonate Ln(III) complexes with heteroaromatic auxiliary ligands: synthesis and luminescence characteristics, *Luminescence*, 2022, **37**, 1921–1931.

61 A. Hooda, A. Dalal, K. Nehra, P. Kumar, D. Singh, R. S. Malik and S. Kumar, Heteroleptic Eu(III) emissive complexes: Luminescent, optoelectronic and theoretical investigation, *J. Lumin.*, 2022, **252**, 119272.

62 L. Zhang, J. Che, Y. Ma, J. Wang, R. Kang, B. Deng and H. Geng, Luminescent and thermal properties of novel orange-red emitting Ca_2MgTeO_6:Sm^{3+} phosphors for white LEDs, *J. Lumin.*, 2020, **225**, 117374.

63 Y. Ma, S. Tang, C. Ji, D. Wu, S. Li, J. Xu and Y. Peng, Sm^{3+} doped novel $Sr_2Ga_2GeO_7$ based high thermal stability red-emitting phosphors for efficient WLED, *J. Lumin.*, 2022, **242**, 118530.